Hindawi
International Journal of Aerospace Engineering
Volume 2022, Article ID 4625001, 17 pages
https://doi.org/10.1155/2022/4625001

Review Article

An Intelligent Trajectory Prediction Algorithm for Hypersonic Glide Targets Based on Maneuver Mode Identification

Mingjie Li,[1] Chijun Zhou,[2] Lei Shao,[2] and Humin Lei[2]

[1]*Graduate College, Air Force Engineering University, Xi'an 710051, China*
[2]*Air and Missile Defense College, Air Force Engineering University, Shanxi, Xi'an 710051, China*

Correspondence should be addressed to Chijun Zhou; zhouchijun666@126.com

Received 25 October 2021; Revised 14 July 2022; Accepted 19 July 2022; Published 22 August 2022

Academic Editor: Jinyang Xu

Trajectory prediction for hypersonic glide targets is a difficult task that needs to be solved. To improve the prediction precision for hypersonic glide targets, based on the analysis of the target's maneuver characteristic, an intelligent trajectory prediction algorithm based on the maneuver mode identification is proposed in this paper. Firstly, according to the typical maneuver modes of the target, a group of parameter suitable for maneuver mode identification and parameter estimation is proposed. The proposed maneuver parameters can reflect the maneuvering characteristics of the target than the other control parameters. Then, the rationality of parameters is analyzed. Secondly, using the long-short-term memory network (LSTM), the structure of intelligent trajectory prediction based on maneuver mode identification is proposed. The proposed prediction method is designed to improve the prediction accuracy by combining the target dynamic model with the flight data. Finally, the maneuver trajectory data set is established to train and test the method. For the test data set, when the observation time for the target is 200 s and the prediction time is 150 s, with a fast prediction speed, our method's average error of spatial distance (AESD) is less than 2.9 km, and the maximum error of spatial distance (MESD) is less than 6.9 km. The result is better than other compared mainstream methods. And it is also proved valid with some observational error.

1. Introduction

Hypersonic glide targets can glide in the near space with a high speed and high mobility. The targets usually have a flight speed higher than Mach 5, a longitudinal maneuverable range of tens of kilometers and a lateral maneuverable range of hundreds of kilometers [1]. Compared with the ballistic target, its longitudinal and lateral maneuverability makes it more difficult to predict its trajectory precisely. Therefore, the trajectory prediction for hypersonic glide targets has been a greater challenge for the interception of interceptors which realize handover between midcourse and terminal guidance according to high probability region prediction [2].

To predict the trajectory of hypersonic glide targets more accurately, the maneuver characteristics of them need to be analyzed. To maximize the longitudinal range and meet the constraints of trajectory points and no-fly zones during flight, a variety of maneuvering modes may be adopted in the trajectory of the target. In the longitudinal direction, according to whether there exists skip glide in the target's trajectory, the modes can be divided into two types: equilibrium and skip glide maneuver. Using optimization methods, Ruan [3] proved that the hypersonic target can reach a larger longitudinal range gliding with the maximum lift-to-drag ratio, while the trajectory is usually not in equilibrium glide maneuver. Ferreira [4] and Chen et al. [5] analyzed the long period trajectory of equilibrium glide first, fitting skip glide maneuver into shock curve by Liouville transformation and general multiple scale theory (GMS) method, and gave the formula for the number of skip maneuver. For the lateral maneuver, the target usually adopts a weaving maneuver and turning maneuver according to the need for penetration. P. Zarcha et al. [6, 7] demonstrated that the target can get rid of the interceptor effectively in the weaving maneuver. T.r. Morris et al. [8, 9] proved that a hypersonic glide target can avoid the no-fly zone by turning maneuver when generating the nominal trajectory. For several maneuver modes, Li

et al. [10] formulated the trajectory expression, deduced the acceleration variation law, and proposed the trajectory generation method considering constraints. The trajectory characteristics in several hypersonic maneuver modes are analyzed in the above literature, which provides the theoretical grounding for our new maneuver parameters to identify maneuver modes in this paper.

According to the prediction mechanism, the current trajectory prediction methods of hypersonic glide targets can be divided into three types: equation analytical method, trajectory fitting method, and control parameter estimation. The equation analytical method can obtain the analytic solution of the target trajectory using the two-body law, which is proved very effective for the ballistic target. However, its only low-order approximate solution can be obtained for an unconventional ballistic target like a hypersonic glide target. Chaptman [11] and Loh et al. [12] et al. proposed approximate analytical solutions of hypersonic target trajectory under certain assumptions. Vinh et al. [13, 14] proposed the second-order approximate solutions of skip glide and equilibrium glide with constant Angle of attack, but the solutions were pretty complex. Lu et al. [15] regarded the quasi-equilibrium glide state of lift vehicles as a regular perturbation problem. The longitudinal trajectory of quasi-equilibrium glide was divided into the combination of equilibrium glide and high-order terms, and the error between the real solution and the low-order solution is discussed. The equation analytic method can obtain a predicted trajectory without the trajectory iteration, which can reach a faster prediction speed. But the precision of this method is restricted because the exact analytical solution cannot be obtained effectively.

The second type is trajectory fitting method, in which linear combination of simple basis functions is used to fit the target trajectory function according to the spatial characteristic of target trajectory [16]. Han et al. [17] established a polynomial model for trajectory of hypersonic glide target and obtained predicted trajectory by estimating the optimal parameters of the polynomial model. In ambition to this, Han et al. [18] also tried to divide the target trajectory directly into several parts without studying the control law and obtained predicted trajectory by fitting the variation law of trajectory state like flight height. The trajectory fitting method performs well when identifying the trajectory characteristics easily, while it is not suited to predict a large number of trajectories in different maneuver modes.

The third type is estimating the control parameter to obtain the predicted trajectory. By fitting the variation law of the key parameters, the predicted trajectory of the target is obtained by integrating from the last observed state. Lei and Han et al. [19, 20] obtained the predicted trajectory through the polynomial fitting of aerodynamic parameters and integrating control parameters with the dynamic model. Li et al. [21] proposed several control laws for different observed trajectories of targets to obtain the predicted trajectory, which could fit the change law of the target's control parameters. Zhai et al. [22] proposed a new control parameter that could reduce the dimensionality of noncooperative target states effectively and fitted in a simple function. The method of estimating control parameters has better prediction accuracy, while the observed state is accurate, and the control law is fitting well. However, the temporal law of the control parameters is usually not a simple function. Improper fitting methods for the parameter will lead to the rapid accumulation of integral errors. Therefore, to improve the prediction precision, a new trajectory prediction method that can provide more prior information and fit the change law of control parameters better is proposed in this paper.

The fitting methods of trajectory prediction for hypersonic glide targets all rely on models or trajectory characteristics, which have a low utilization rate of flight data. However, in recent years, data-driven temporal sequential prediction methods have obtained good effects [23, 24], by which the trajectories of reentry glide targets can be predicted with the help of flight data. On the other hand, in recent years, deep learning technology has shown strong advantages in temporal law prediction [25] and target recognition [26], which had been widely used in vessel trajectory prediction [27, 28] and vehicle trajectory prediction [29]. Especially, several complicated temporal sequential prediction problems have been solved based on the recurrent neural network (RNN), which has shown the powerful studying ability of data. For example, Kailiu et al. [30] combined long- and short-term memory networks (LSTM) and the Gaussian process regression method (GPR) to predict battery capacity and service life in the future accurately. At the same time, a RNN framework is designed to obtain an effective daily capacity prediction value whether storage of battery has been observed [31]. And the neural networks also were applied to hypersonic trajectory prediction. Yang et al. [32] modified the trajectory prediction error based on the generalized regression neural network (GRNN), by which the accurately predicted trajectory could be obtained. Li et al. [33] combined the neural network and Kalman filter, based on the filtering result obtained the predicted trajectory. Cai et al. [34] established trajectory data sets of different maneuver modes for hypersonic targets and realized the classification and prediction of hypersonic glide target trajectory by using LSTM. Xie et al. [35] designed a gated recurrent unit (GRU) based on a double-channel neural network and proposed a trajectory data set. According to the network, the predicted trajectories of the hypersonic glide target were obtained. All the above methods regard the prediction of the target's trajectory state as the prediction of a temporal sequence and use a temporal neural network to learn the state's variation law. However, these methods cannot make full use of the information of the observed target, which lacks a combination with the target's dynamic model.

1.1. Motivation and Contribution. Identifying the maneuver modes of the target accurately is helpful to trajectory prediction. And considering using a temporal neural network to learn the temporal law of the target's control parameters may obtain better results than fitting with a simple function, an intelligent trajectory prediction algorithm for hypersonic glide targets is proposed in this paper, which is based on maneuver mode identification by combining LSTM with maneuver parameter model. Compared with the traditional

trajectory prediction of hypersonic glide targets, the flight data are used to improve the accuracy of maneuver mode identification and trajectory prediction. And compared with the data-driven prediction methods, the dynamic models and maneuver characteristics are used to provide more information for prediction.

In this paper, the dynamic models and common maneuver modes of hypersonic glide targets are given firstly. According to the trajectory characteristics in different maneuver modes, a group of maneuver parameters suitable for maneuver mode identification and parameters estimation is proposed, when the rationality of parameters is deduced. Then, an intelligent trajectory prediction algorithm based on maneuver mode identification is proposed, which consists of the initial and last point modification network, maneuver parameters modification network, and prediction network. By generating and learning the hypersonic target trajectory data set, our method can predict the trajectory of the target effectively and obtains excellent prediction precision. In the case of the observation time is 200 s and the prediction time is 150 s, the prediction accuracy of our model reaches 98.63%, the prediction consuming time is about 0.0105 s, the average error of spatial distance (ASDE) is less than 2.64 km, and the maximum error of spatial distance (MSDE) is less than 6.91 km. And it is proved valid with the larger observational error. Finally, compared with some mainstream prediction methods, the simulation results show that our method has better prediction precision.

The innovation of this paper can be summarized in several points:

(1) A new group of maneuver parameters is proposed, which is easier to be estimated and to identify the maneuver modes. And its rationality is analyzed according to the dynamic models of the hypersonic glide target

(2) An intelligent trajectory prediction algorithm for hypersonic glide targets based on maneuver mode identification is proposed, and the algorithm's framework, process, and training loss function are introduced

(3) The data set for the trajectory of hypersonic glide targets in different maneuvers is established, based on which several neural networks in the algorithm are trained and tested. The ablation experiment results of each partial network in the algorithm are shown when the experiment results with different observational errors are shown. And the prediction results of our method are compared with part of the current trajectory prediction algorithms

1.2. Organization. This paper is organized as follows: Section 1 introduces the research status of maneuvering characteristics and trajectory prediction of hypersonic glide targets when the work of this paper is introduced briefly. Section 2 provides the dynamic model and common maneuver modes of hypersonic glide targets; then, definition and analysis of maneuver parameter are introduced. Section 3 provides the framework and process of our trajectory prediction algorithm. In Section 4, the simulation data set is constructed, and the simulation result is shown. Conclusions are drawn in Section 5.

2. The Dynamic Model of Hypersonic Glide Target and Analysis of Parameters

2.1. Dynamic Models of Hypersonic Glide Targets. Using the earth-centered earth-fixed coordinate (ECFG), east-north-up (ENU) coordinate, velocity-turning-climb (VTC) coordinate, and geographic coordinate, based on simple atmospheric and gravity models, while ignoring the effect of earth rotation, the dynamic model of hypersonic glide targets can usually be shown as

$$\begin{cases} \dot{h} = v \sin\theta \\ \dot{\phi} = \dfrac{v \cos\theta \sin\psi}{(R_e + h)\cos\varphi} \\ \dot{\varphi} = \dfrac{v \cos\theta \cos\psi}{(R_e + h)} \\ \dot{v} = -\dfrac{D}{m} - g \sin\theta \\ \dot{\theta} = \dfrac{L \cos\beta}{mv} + \cos\theta\left(\dfrac{v}{R_e + h} - \dfrac{g}{v}\right) \\ \dot{\psi} = \dfrac{L \sin\beta}{mv \cos\theta} + \dfrac{v \cos\theta \sin\psi \tan\varphi}{R_e + h} \end{cases}, \tag{1}$$

where h is the flight height of target, ϕ is the longitude of target, φ is the latitude of target, v is the speed of target, θ is the path angle of target,ψ is the heading angle of target, L is the lift on the target, D is the drug on the target, and R_e is the earth radius.

Switch the state of the target to the ENU coordinate, when $h << \mathrm{Re}$, the new state of the target can be shown as $S = [X, Y, Z, \dot{X}, \dot{Y}, \dot{Z}]$.

$$\begin{cases} X = \phi R_e \\ Y = \varphi R_e \\ Z = h \\ \dot{X} = v \sin\psi \cos\theta \\ \dot{Y} = v \cos\psi \cos\theta \\ \dot{Z} = v \sin\theta \end{cases}, \tag{2}$$

where X is the east position of target in ENU, Y is the north position of target in ENU, and Z is the up position of target in ENU.

In general, the dynamic model of the hypersonic glide targets can be transformed into

$$\dot{\boldsymbol{x}}(t) = \begin{bmatrix} \mathbf{0}_{3\times3} & \mathbf{I}_{3\times3} \\ \mathbf{0}_{3\times3} & \mathbf{0}_{3\times3} \end{bmatrix} \boldsymbol{x}(t) + \begin{bmatrix} \mathbf{0}_{3\times3} \\ \mathbf{I}_{3\times3} \end{bmatrix} \left(\frac{1}{2}\rho V^2 \mathbf{T}_{\mathrm{VTC}}^{\mathrm{ENU}} \begin{bmatrix} \xi_v(t) \\ \xi_t(t) \\ \xi_c(t) \end{bmatrix} + \boldsymbol{g}(t) \right), \tag{3}$$

where ξ_v, ξ_t, ξ_c are the aerodynamic parameters of target in VTC coordinate.

2.2. Analysis for Maneuver Modes of Hypersonic Glide Targets. According to literature [10], hypersonic glide targets have several maneuver modes in the longitudinal and lateral directions. Lateral maneuvers usually contain weaving maneuver and turning maneuver, and longitudinal maneuvers usually contain equilibrium glide and skip glide. The definition is shown as follows:

2.2.1. Longitudinal Maneuver. If the target is in equilibrium glide maneuver mode, it must meet

$$\dot{\theta} = \frac{L\cos\beta}{\mathrm{mv}} + \cos\theta\left(\frac{v}{R_e + h} - \frac{g}{v}\right) = 0. \tag{4}$$

In general, $\cos\theta \approx 1$ if target is in equilibrium glide maneuver mode. And the equilibrium glide maneuver equation can be simplified as $L\cos\beta/m = g - v^2/\mathrm{Re} + h$. If the target's aerodynamic force meets this equation, it is in the equilibrium glide maneuver mode. Otherwise, the target's trajectory appears as a skip glide. According to the common guidance methods of hypersonic glide targets, an attack angle profile is usually designed to finish the longitudinal guide. By the attack angle profile, the target can finish the skip glide with longer range when constraints are met.

2.2.2. Lateral Maneuver. The trajectory in lateral maneuver mode of hypersonic glide targets usually contains weaving maneuver and turning maneuver. And the weaving maneuver can be expressed as follows:

$$l = \frac{l_0 + l_b(b)}{2 \cdot \sin\left(\omega(b)b + w(b)\right)}, \tag{5}$$

where l_0 is the base line position of weaving maneuver mode, l_b is the range of maneuver mode, ω is the frequency of weaving, and w is the initial phase position.

The trajectory in turning maneuver mode is usually a monotonous curve line that can be expressed by polynomial functions.

$$l = \sum_{i=0}^{N} f_i b^i, \tag{6}$$

where f_i is constants coefficient and the trajectory meets dl /db < 0 or dl/db > 0.

2.3. Analysis of Maneuver Parameter Model. According to the analysis in Section 2.2, there are four typical types of longitudinal and lateral maneuver modes for hypersonic glide targets. And based on the analysis of maneuver characteristics, it is found that the longitudinal maneuver mode's identification mainly depends on whether the longitudinal equilibrium equation can be satisfied. What is more, the lateral maneuver mode identification depends on the functional relation between lateral and baseline trajectory. Therefore, the original parameter relation of the ENU coordinate is transformed in this section.

Assuming that the aerodynamic parameters of the target in the ENU coordinate are $\xi_e(t), \xi_n(t), \xi_u(t)$, The functional relation between ξ_e, ξ_n, ξ_u and ξ_v, ξ_t, ξ_c is

$$\begin{bmatrix} \xi_d(t) \\ \xi_t(t) \\ \xi_c(t) \end{bmatrix} = \mathbf{T}_{\mathrm{ENU}}^{\mathrm{VTC}} \begin{bmatrix} \xi_e(t) \\ \xi_n(t) \\ \xi_u(t) \end{bmatrix}, \tag{7}$$

where $\mathbf{T}_{\mathrm{ENU}}^{\mathrm{VTC}}$ is the transformation matrix between ENU and VTC coordinate.

And assuming the included angle between the baseline direction of the target and the longitudinal direction (east) is σ, the parameters of the target in the baseline, lateral, and up direction are $\xi_b(t), \xi_l(t), \xi_u(t)$, and then, the function relation between ξ_b, ξ_l, ξ_u and ξ_e, ξ_n, ξ_u is

$$\begin{bmatrix} \xi_b(t) \\ \xi_l(t) \\ \xi_u(t) \end{bmatrix} = \begin{bmatrix} \cos\sigma & \sin\sigma & 0 \\ -\sin\sigma & \cos\sigma & 0 \\ 0 & 0 & 1 \end{bmatrix}^{-1} \begin{bmatrix} \xi_e(t) \\ \xi_n(t) \\ \xi_u(t) \end{bmatrix} = \left[T_{\mathrm{AX}}^{\mathrm{ENU}}\right]^{-1} \begin{bmatrix} \xi_e(t) \\ \xi_n(t) \\ \xi_u(t) \end{bmatrix}, \tag{8}$$

where $\mathbf{T}_{\mathrm{AX}}^{\mathrm{ENU}}$ is the transformation matrix between baseline coordinate and ENU coordinate.

Therefore, the dynamic equation of the target can be expressed as

$$\dot{x}(t) = \begin{bmatrix} 0_{3\times3} & I_{3\times3} \\ 0_{3\times3} & 0_{3\times3} \end{bmatrix} x(t) + \begin{bmatrix} 0_{3\times3} \\ I_{3\times3} \end{bmatrix} \left(\frac{1}{2}\rho V^2 T_{\mathrm{AX}}^{\mathrm{ENU}} \begin{bmatrix} \xi_b(t) \\ \xi_l(t) \\ \xi_u(t) \end{bmatrix} + g(t) \right), \tag{9}$$

where ρ is the atmospheric density and $I_{3\times3}$ is the standard matrix whose size is 3×3.

Let $\xi_{uq} = \xi_u - g/q$, the baseline-lateral-up coordinate is called the BLU coordinate, and the aerodynamic acceleration in the BLU coordinate can be expressed as

$$\begin{bmatrix} a_b \\ a_l \\ a_u \end{bmatrix} = \frac{1}{2}\rho V^2 \begin{bmatrix} \xi_b \\ \xi_l \\ \xi_{\mathrm{uq}} \end{bmatrix}. \tag{10}$$

The dynamic model of the hypersonic glide targets can be transformed as

$$\begin{cases} \dot{h} = V\sin\theta \\ \dot{\phi} = \dfrac{V\cos\theta\sin\psi}{(R_e+h)\cos\varphi} \\ \dot{\varphi} = \dfrac{V\cos\theta\cos\psi}{R_e+h} \\ \dot{V} = -\dfrac{(\cos\Delta\delta\sin\psi\cos\theta+\sin\Delta\delta\cos\theta)\xi_b}{2}\rho V^2 + \\ \dfrac{(\cos\Delta\delta\cos\psi\cos\theta-\sin\Delta\delta\sin\psi)\xi_l+\cos\Delta\delta\sin\theta\xi_u}{2}\rho V^2 - g\sin\theta \\ \dot{\theta} = \dfrac{((\sin\psi\sin\psi_b-\cos\psi_b\cos\psi)\xi_b+(\sin\psi\sin\psi_b+\cos\psi\cos\psi_b))\xi_l\rho V}{2} + \\ \cos\theta\left(\dfrac{V}{R_e+h}-\dfrac{g}{V}\right) \\ \dot{\psi} = \dfrac{(-\sin\psi\sin\psi_b\sin\theta-\cos\psi\cos\psi_b\sin\theta)\xi_b\rho V+}{2\cos\theta} + \\ \dfrac{((\sin\psi\cos\psi_b\sin\theta-\cos\psi\sin\psi_b\sin\theta)\xi_l+\cos\theta\xi_u)\rho v}{2\cos\theta} + \dfrac{V\cos\theta\sin\psi\tan\varphi}{R_e+h} \end{cases}, \tag{11}$$

where ψ_b is the heading angle of the baseline.

According to the definition of lateral maneuver in Section 2.2, the lateral maneuver distance often can be thought to have a certain functional relation with the baseline distance, which is more obvious in the lateral curvature. If the target's lateral maneuver mode is weaving maneuver, the lateral curvature can still be seen as a sine function. And if the target's lateral maneuver mode is turning maneuver, the lateral curvature r_a can still be seen as a polynomial function whose order decreases. The functional relation between r_a and ξ_b, ξ_l is

$$\begin{aligned} r_a &= \frac{d^2l}{db^2} = \frac{l''b'-b''l'}{b'^3} \\ &= \frac{\rho}{2}\frac{V^2\xi_l v\cos\theta\cos\Delta\psi - V^2\xi_b v\cos\theta\sin\Delta\psi}{V^3\cos^3\theta\cos^3\Delta\psi}, \\ &= \frac{\rho}{2}\frac{\xi_l\cos\Delta\psi-\xi_b\sin\Delta\psi}{\cos^2\theta\cos^3\Delta\psi} \end{aligned} \tag{12}$$

where $\Delta\psi$ is the difference value between the yaw angle of the target with the baselines.

2.3.1. Analysis of Longitudinal Maneuver Parameters.

$$\xi_{\mathrm{uq}} = \frac{\ddot{Z}}{q} = \frac{\ddot{h}}{q} = (v\sin\theta)' = \dot{v}\sin\theta + \dot{\theta}v\cos\theta. \tag{13}$$

When the target's longitudinal maneuver is equilibrium glide, $\dot{\theta}=0$, θ is unchanged and close to 0. Then, $\xi_{\mathrm{uq}} = \dot{v}\sin\theta = (D/m - g\sin\theta)\sin\theta/q \approx D\theta/\mathrm{mq} = \xi_d\theta$, and ξ_{uq} changes stably and smoothly. The result of ξ_{uq} changes is shown in Figure 1(a). For skip glide, $\dot{\theta}$ is a fluctuation value between the positive value and the negative value. Because $v\cos\theta$ is always a positive value, $\dot{\theta}v\cos\theta$ can be regarded as a vibration term added on the previous term, and skip glide's result is shown in Figure 1(b). As shown in Figure 1, the ξ_{uq} in equilibrium glide mode changes smoothly. However, it is more likely that the wave effect added on the smooth curve in skip glide mode.

2.3.2. Analysis of Lateral Maneuver Parameter. Because the initial position and baseline direction of the target's trajectory cannot be effectively inferred from the observation data, therefore, the initial velocity direction of the first observation point is chosen to replace the baseline direction in this paper. The rationality is analyzed as follows:

(1) The Rationality for Weaving Maneuver. For weaving maneuver, $l \ll b$, and the overload of hypersonic glide targets is limited, and its lateral velocity increases slowly and far less than the baseline velocity, so dl/db is close to 0. The offset between the first observation point's velocity direction with the baseline direction is a small value.

Assuming the first observation point position is (x_0, y_0), the heading angle is σ. And the actual heading angle of baseline direction is $\sigma + \Delta\sigma$. $\Delta\sigma$ is a small value, so the following function relation exists

$$\begin{bmatrix} \cos\sigma & -\sin\sigma \\ \sin\sigma & \cos\sigma \end{bmatrix}\begin{bmatrix} y-y_0 \\ x-x_0 \end{bmatrix} = \begin{bmatrix} l \\ b \end{bmatrix}, \tag{14}$$

where l is the lateral position of target in the actual BLU coordinal and b is the longitudinal position in the actual BLU coordinal.

If regard the first observation point as the initial position of target, then

$$\begin{bmatrix} \cos(\sigma+\Delta\sigma) & -\sin(\sigma+\Delta\sigma) \\ \sin(\sigma+\Delta\sigma) & \cos(\sigma+\Delta\sigma) \end{bmatrix}\begin{bmatrix} y \\ x \end{bmatrix} = \begin{bmatrix} l' \\ b' \end{bmatrix}, \tag{15}$$

where l' is the lateral position of the target in the observation BLU coordinal and b' is the longitudinal position in the observation BLU coordinal.

Because $\Delta\sigma$ is a small value and $l \ll b$

$$\begin{aligned} \begin{bmatrix} l' \\ b' \end{bmatrix} &\approx \begin{bmatrix} \cos\sigma(y-y_0)-\sin\sigma(x-x_0)-\Delta\sigma(\sin\sigma(y-y_0)+\cos\sigma(x-x_0))+ \\ (y_0\cos\sigma+x_0\sin\sigma-\Delta\sigma\sin\sigma y_0-\Delta\sigma\cos\sigma x_0) \\ \sin\sigma(y-y_0)+\cos\sigma(y-y_0)+\Delta\sigma(\cos\sigma(y-y_0)-\cos\sigma(x-x_0))+ \\ (y_0\sin\sigma+x_0\cos\sigma+\Delta\sigma\cos\sigma y_0-\Delta\sigma\sin\sigma x_0) \end{bmatrix}, \\ &= \begin{bmatrix} l-\Delta\sigma b+(y_0\cos\sigma+x_0\sin\sigma-\Delta\sigma\sin\sigma y_0-\Delta\sigma\cos\sigma x_0) \\ b+\Delta\sigma l+(y_0\sin\sigma+x_0\cos\sigma+\Delta\sigma\cos\sigma y_0-\Delta\sigma\sin\sigma x_0) \end{bmatrix}, \\ &\approx \begin{bmatrix} l-\Delta\sigma b+(y_0\cos\sigma+x_0\sin\sigma-\Delta\sigma\sin\sigma y_0-\Delta\sigma\cos\sigma x_0) \\ b+(y_0\sin\sigma+x_0\cos\sigma+\Delta\sigma\cos\sigma y_0-\Delta\sigma\sin\sigma x_0) \end{bmatrix}. \end{aligned} \tag{16}$$

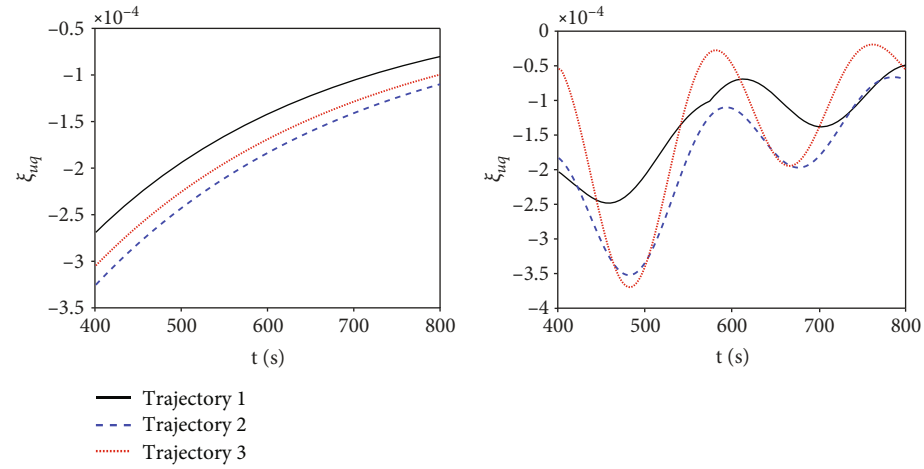

FIGURE 1: The variation of ξ_{uq}. (a) is the variation of ξ_{uq} in equilibrium glide, and (b) is the variation of ξ_{uq} in skip glide.

Then,

$$\begin{aligned}\frac{d^2l'}{db'^2} &= \frac{d\left(dl'/dt\right)\left(dt/db'\right)}{dt}\frac{dt}{db} \\ &= \frac{\ddot{l}'\dot{b}' - \ddot{b}'\dot{l}'}{\dot{b}'^3} \\ &\approx \frac{\left(\ddot{l} - \Delta\sigma\dddot{b}\right)\dot{l} - \left(\dot{l} - \Delta\sigma\ddot{b}\right)\ddot{l}}{\dot{l}^3} \\ &= \frac{\dddot{b}\dot{l} - \ddot{b}\ddot{l}}{\dot{l}^3} \\ &= \frac{d^2l}{db^2}.\end{aligned} \tag{17}$$

Therefore, trajectory curvature for weaving maneuver can be simplified as

$$r_a = \frac{\rho}{2}\frac{\xi_l}{\cos^2\theta}. \tag{18}$$

The curvature effect of weaving maneuver is shown in Figure 2. As shown in Figure 2, r_a changes between positive with negative value, and its change looks like a sinusoidal curve can be identified easily.

(2) The Rationality of Turning Maneuver. According to the definition of turning maneuver, the expression of turning maneuver is $l = \sum_{i=1}^{n} f_i b^i$, and $\dot{l}(b) > 0$ or $\dot{l}(b) < 0$, the sign of trajectory curvature K does not change. K is expressed as follows:

$$K = \frac{\ddot{l}}{\left(1 + \dot{l}^2\right)^{3/2}}. \tag{19}$$

Therefore, when the curvature's sign does not change, we can obtain

$$\begin{cases} \ddot{l} \le 0, \text{ if } \dot{l} < 0 \\ \ddot{l} \ge 0, \text{ if } \dot{l} > 0 \end{cases}. \tag{20}$$

As shown in Figure 3, a new $B'L'U$ coordinate is established from the first observation point. And the observation position in the new coordinate is

$$\begin{bmatrix} b' \\ l' \end{bmatrix} = \frac{1}{\sqrt{1 + \dot{l}_0^2}}\begin{bmatrix} 1 & \dot{l}_0 \\ -\dot{l}_0 & 1 \end{bmatrix}\begin{bmatrix} \Delta b \\ l - l_0 \end{bmatrix} = \begin{bmatrix} \dfrac{\Delta b + \dot{l}_0(l - l_0)}{\sqrt{1 + \dot{l}_0^2}} \\ \dfrac{-\dot{l}_0\Delta b + (l - l_0)}{\sqrt{1 + \dot{l}_0^2}} \end{bmatrix}, \tag{21}$$

where l_0 is the longitudinal position of the target in the original BLU coordinate, and Δb is the difference value between the target lateral position with the first observation point's lateral position in the original BLU coordinate.

Due to the sign of $\dot{l}$ which does not change in the turning maneuver, $\dot{l}(l - l_0)$ is always greater than 0. Assuming there will be no turning and turning trajectory during the turning trajectory, let $\dot{l} > 0, \ddot{l} > 0$ in the original design trajectory. And because

$$\frac{dl'}{db'} = \frac{\dot{l} - \dot{l}_0}{1 + \dot{l}_0\dot{l}} > 0, \tag{22}$$

$$\frac{d^2l'}{db'^2} = \frac{\ddot{l}\left(1 + \dot{l}_0^2\right)^{3/2}}{\left(1 + \dot{l}\dot{l}_0\right)^3} = \frac{\ddot{l}}{\left(1 + \dot{l}\dot{l}_0\right)^{3/2}}\frac{\left(1 + \dot{l}_0^2\right)^{3/2}}{\left(1 + \dot{l}\dot{l}_0\right)^{3/2}}. \tag{23}$$

Then, we can obtain

$$\frac{\ddot{l}}{\left(1+\dot{l}_0^{\,2}\right)^{3/2}} \geq \frac{d^2 l'}{\mathrm{db}'^2} \geq \frac{\ddot{l}}{\left(1+\dot{l}^2\right)^{3/2}} \frac{\left(1+\dot{l}_0^2\right)^{3/2}}{\left(1+\dot{l}^2\right)^{3/2}} = K_{b'} \frac{\left(1+\dot{l}_0^2\right)^{3/2}}{\left(1+\dot{l}^2\right)^{3/2}} > 0. \tag{24}$$

Therefore, fitting the lateral trajectory in the $B'L'U$ coordinate by a polynomial function, the trajectory can still be regarded as a turning maneuver according to the definition. For the turning maneuver, the curvature r_a is expressed as follows:

$$r_a = \frac{\rho}{2} \frac{\xi_l \cos \Delta\sigma - \xi_b \sin \Delta\sigma}{\cos^2\theta \cos^3 \Delta\delta}. \tag{25}$$

The variation of curvature r_a is shown in Figure 4. Figures 4(a) and 4(b) represent the variation of parameters r_a in longitudinal equilibrium and skip glide modes. For turning maneuver, the lateral overload of the hypersonic glide target is limited, so the trajectory curvature is a small value. Because the target's state is coupled to the overload constraint, its flight trajectory is influenced by the longitudinal maneuver mode, even so r_a can still keep stable within a certain range and its variation is smooth.

In conclusion, according to the variation of $\xi_b, r_a, \xi_{\mathrm{uq}}$, the maneuver modes of the target can be identified effectively. According to the definition of maneuver, if the trajectory of weaving maneuver contains sine term, r_a is still the sine function of b. If the trajectory is in turning maneuver mode, its lateral design function is usually a high-order polynomial function. Obtained predicted trajectory by r_a can reduce the function's order effectively. Based on the parameters ξ_b, r_a, ξ_{uq}, an intelligent trajectory prediction for hypersonic glide targets is designed in Section 3.

3. Intelligent Trajectory Prediction Algorithm Based on Maneuver Mode Identification

In the above section, the maneuver parameters $\xi_b, r_a, \xi_{\mathrm{uq}}$ are deduced, and the rationality of them has been analyzed. Therefore, an intelligent trajectory prediction algorithm for hypersonic glide targets based on maneuver mode identification is proposed in this section.

3.1. LSTM Neural Network. The long and short temporal memory neural network (LSTM) is specially designed to solve temporal sequence problems. The unit of LSTM contains forgetting gate, input gate, and output gate, several three gates structures, which can protect and control the temporal information more effectively than the common unit structure of RNN. The structure of LSTM unit is shown in Figure 5.

In Figure 5, f_t is the forgetting gate; $f_t = \delta(W_f \cdot [h_{t-1}, x_t] + b_f)$. Forgetting gate reads the output of the previous unit and the input of the current unit. δ is the sigmoid function, and W_f, b_f are the network parameters of forgetting gate. $\tilde{C}_t = \tanh(W_i \cdot [h_{t-1}, x_t] + b_i)$ and $i_t = \delta(W_i \cdot [h_{t-1}, x_t] + b_i)$ constitute the input gate, where W_f, b_f are the network parameters of the input gate. i_t determines the information to be updated, and $\tilde{C}_t$ generates the vector to select the content to be updated and finally update the unit state combining with two parts; $o_t = \delta(W_o \cdot [h_{t-1}, x_t] + b_o)$, $h_t = o_t \cdot \tanh(C_t)$ is the output value of the out gate, where W_o, b_o are the network parameters of output gate. The output gate determines the output content. LSTM network has an excellent memory and learning ability for temporal information and can extract and fit temporal law effectively. Using the LSTM network and maneuver parameters model, a trajectory prediction algorithm based on maneuver mode identification is proposed in this paper.

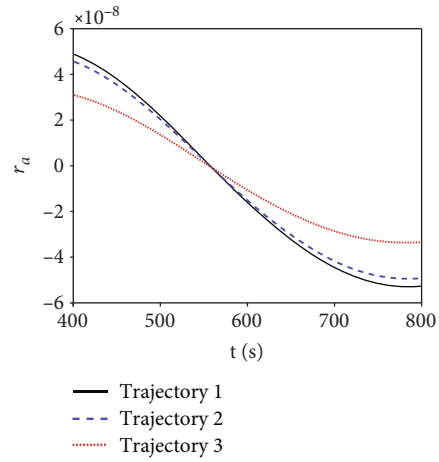

Figure 2: Variation of r_a in the weaving maneuver mode.

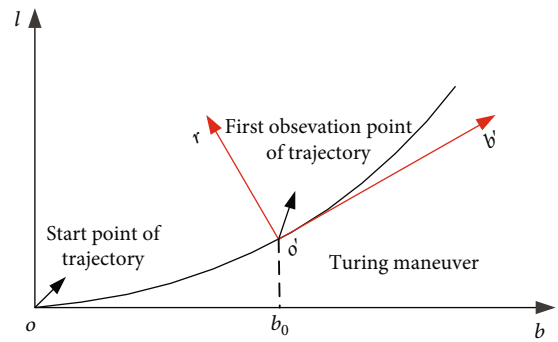

Figure 3: New maneuver coordinate$B'L'U$.

3.2. Intelligent Trajectory Prediction Algorithm. From the analysis in Section 2.3, the function relation between r_a with ξ_l is

$$\frac{2r_a \cos^2\Delta\sigma \cos^2\theta}{\rho} + \xi_b \tan \Delta\sigma = \xi_l. \tag{26}$$

For different maneuver modes, there are different equations with prior information that can be used to predict trajectory. The transformation relationship of different maneuver modes is shown in Table 1.

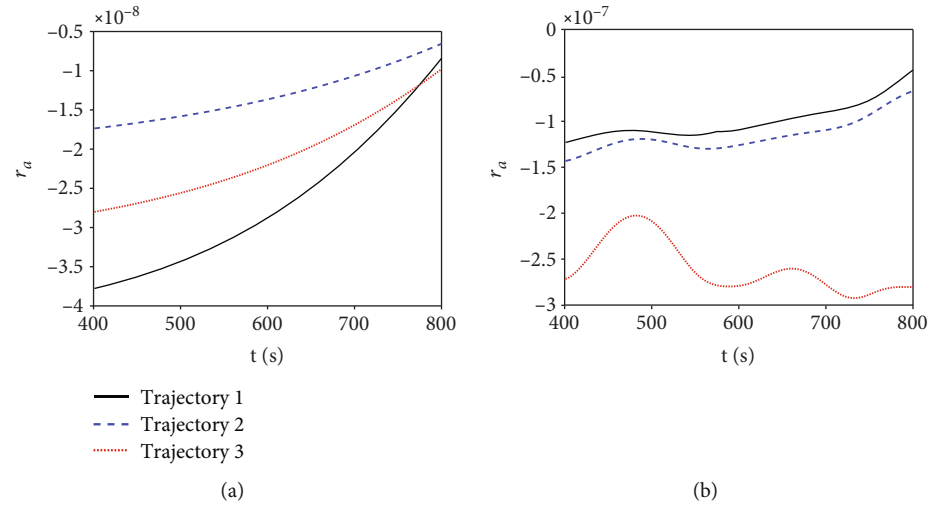

Figure 4: The variation of r_a in turning maneuver mode. (a) is the variation of r_a in equilibrium glide. (b) is the variation of r_a in skip glide.

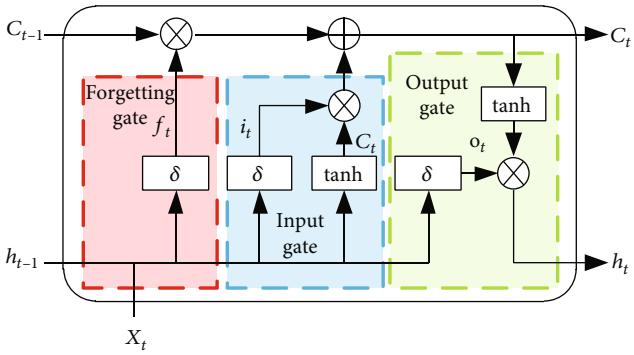

Figure 5: The unit of LSTM.

Table 1: Transformation relationship table.

Maneuver mode	Transformation relationship and prior knowledge
Weaving equilibrium glide	$2r_a/\rho = \xi_l,\ \dot{\theta} = 0$
Weaving skip glide	$2r_a \cos^2\theta/\rho = \xi_l$
Turing equilibrium glide	$2r_a \cos^2\Delta\sigma/\rho + \xi_b \tan\Delta\sigma = \xi_l,\ \dot{\theta} = 0$
Turning skip glide	$2r_a \cos^2\Delta\sigma \cos^2\theta/\rho + \xi_b \tan\Delta\sigma = \xi_l$

As shown in Table 1, the dynamic models of different maneuver modes differ greatly. It means that the prediction precision can be improved when the maneuver mode of target is identified before predicting trajectory. What is more, the lateral and longitudinal maneuver modes of the target can be identified by estimating the three maneuver parameters $[\xi_b, r_a, \xi_{uq}]$, and the predicted trajectory can be obtained through prior information with Equation (11).

3.2.1. Structure of Trajectory Prediction Algorithm

(1) Initial and Last Point Modification Network $\varphi_{il}(\cdot)$. The prediction algorithm in this paper makes the first observation point and its velocity direction the initial position and baseline direction. Therefore, the velocity direction of the initial point must be accurate enough. On the other hand, for the trajectory prediction using integration, the initial point's state of integration has a great influence on the prediction accuracy. The original data and observation data were brought into the initial and last point modification network to modify the positions of the observed initial and last point position. The size of the LSTM network is $[6, 128, 2]$. The observed normalized initial and last point 6-dimensional sequence $[R_{oi}, \phi_{oi}, \varphi_{oi}, v_{oi}, \theta_{oi}, \psi_{oi}]$ and $[R_{ol}, \phi_{ol}, \varphi_{ol}, v_{ol}, \theta_{ol}, \psi_{ol}]$ are brought into the LSTM network, which has 2 layers with 128 intermediate nodes. Then, connect to the fully connected network for training. The initial and last point modification network is used to obtain the direction of modified observation initial point heading angle ψ_{bm} and modified observation last point state $[R_l, \phi_l, \varphi_l, v_l, \theta_l, \psi_l]$.

(2) Maneuver Parameter Modification Network $\varphi_m(\cdot)$. Due to the error of the filtering algorithm, the variation of the maneuver parameters obtained by filtering is not smooth. Therefore, the error of directly applying the maneuver parameter obtained by filtering into the temporal sequence prediction network is pretty large. The original maneuver parameter data and filtering maneuver parameter data are brought into the parameter modification network, which can modify and smooth the variation of maneuver parameters. The size of the LSTM network is $[3, 128, 2]$. Then, connect to the fully connected network. The normalized maneuver parameter data after filtering $\xi_b^f, r_a{}^f, \xi_{uq}^f$ are brought into the parameter modification network for training, and the modified maneuver parameter data $\xi_b^m, r_a{}^m, \xi_{uq}^m$ are obtained.

(3) Prediction Network. This network is used to learn temporal sequence relationships from a large number of original maneuver parameter data and predicted maneuver parameters in the future. The presegment and postsegment maneuver data are brought into the network to learn their temporal sequence relationship. Similarly, the size of LSTM is [3, 128, 2]. Then, connect to the full connection network. The network can predict the maneuver mode of the target m_p and maneuver parameters $\xi_b^p, r_a{}^p, \xi_{\text{uq}}^p$ in the future.

The trajectory prediction structure based on maneuver identification is shown in Figure 6, and the process of prediction is as follows:

3.2.2. Data Normalization. In order to improve the learning efficiency of the network, the observation data is normalized first. Then, the upper and lower limits of all kinds of data $X_{\max}, X_{\min}$ are obtained by using the original data of all trajectories, and the data is normalized as

$$X' = \frac{X - X_{\min}}{X_{\max} - X_{\min}}. \tag{27}$$

Through the normalization operation, all the data can be transformed into $[0, 1]$, which is convenient for network training.

3.2.3. Modification of the Initial and Last Point Position. The normalized position of the observation initial and last point is put into the start and last point modification network to calculate the baseline direction and the position of the modified last point.

$$\psi_{\text{bm}}, S_l = \varphi_{\text{il}}(S_o). \tag{28}$$

3.2.4. Modification of Maneuver Parameters. Use the tracking algorithm to deal with the observation data to obtain the filtering data$S_f = [R_f, \phi_f, \varphi_f, V_f, \theta_f, \psi_f]$. Then, the new filtering maneuver parameters $\xi^f = \xi_b^f, r_a{}^f, \xi_{\text{uq}}^f$ are calculated according to the dynamic model M. The filtering parameters are sent into the maneuver parameter modification network $\varphi_m(\cdot)$ to obtain the modified maneuver parameters $\xi^m = \xi_b^{\text{m}}, r_a{}^m, \xi_{\text{uq}}^m$.

$$\xi^m = \varphi_m\left(\xi^f\right). \tag{29}$$

3.2.5. Trajectory Prediction. According to the temporal law of the modified parameters $\xi_b^m, r_a{}^m, \xi_{\text{uq}}^m$, predict the longitudinal, lateral maneuver mode, and maneuver parameter's variation law using the prediction network. According to the equation in Table 1, the more accurate parameter ξ_l^m is obtained. Finally, the trajectory of target $S_p = [R_p, \phi_p, \varphi_p, V_p, \theta_p, \psi_p]$ is extrapolated integrally with the dynamic model and the modified position.

$$S_p = M\left(S_l, \psi_{\text{bm}}, \xi_p\right). \tag{30}$$

3.3. The Loss of Algorithm. Prediction loss l contains three parts: the loss of initial and last point modification network loss l_{il}, the loss of maneuver parameter modification network l_m, and the loss of prediction network l_p, where the loss of prediction network loss $l_p = l_{\text{cls}} + l_{\text{reg}}$ and $l_{\text{cls}}, l_{\text{reg}}$ represent the loss of mode identification network and the loss of maneuver parameter prediction network. The mean square error is used for the initial and last point modification network, the loss of parameter maneuver parameter modification network, and the loss of the prediction network. What is more, the cross-entropy loss is used for the mode identification network. The formulas of loss are shown as follows:

$$l_{\text{if}} = \sqrt{\frac{\sum_i^N \left(S_{\text{mlli}} - S_{\text{olli}}\right)^2}{N}} + \sqrt{\frac{\sum_i^N \left(S_{\text{mili}} - S_{\text{oili}}\right)^2}{N}}, \tag{31}$$

$$l_m = \sqrt{\frac{\sum_i^N \left(\xi_{\text{mi}} - \xi_{\text{fi}}\right)^2}{N}}, \tag{32}$$

$$l_{\text{reg}} = \sqrt{\frac{\sum_i^N \left(\xi_{\text{pi}} - \xi_{\text{di}}\right)^2}{N}}, \tag{33}$$

$$l_{\text{cls}} = -[l_{\text{cls}} \log p_{\text{cls}} + (1 - l_{\text{cls}}) \log p_{\text{cls}}], \tag{34}$$

where $S_{\text{mili}} S_{\text{mlli}}$ represent the position of the $i-$th predicted start point and last point in a batch, $S_{\text{oili}} S_{\text{olli}}$ represent the position of the $i-$th observed start point and last point in a batch, and N represents the number of batches in Equation (31); ξ_{mi} is the $i-$th modified maneuver parameter sequence in a batch, and ξ_{fi} is the $i-$th filtering maneuver parameter sequence in a batch in Equation (32); ξ_{pi} is the $i-$th modified maneuver parameter sequence in a batch, and ξ_{di} is the $i-$th generated maneuver parameter sequence in a batch in Equation (33). $l_{\text{cls}}, p_{\text{cls}}$, respectively, represent the one-hot value of label classification and prediction classification in Equation (34).

4. Simulation

4.1. Maneuver Trajectory Data Set. According to the definition of hypersonic maneuver modes in 2.2, two maneuver modes in the longitudinal direction are designed is this section by using the equilibrium equation and attack angle profile, when the weaving and turning maneuver trajectory in the lateral direction are also designed. The specific formula is shown in Table 2.where $\alpha - v$ is the attack angle-velocity profile. Because the hypersonic glide target has a high initial speed, a high angle of attack is usually be using in the start stage, which can reduce the heat flux density of the target to meet the constraints. On the other hand, to reach the maximum longitudinal range, hypersonic glide targets

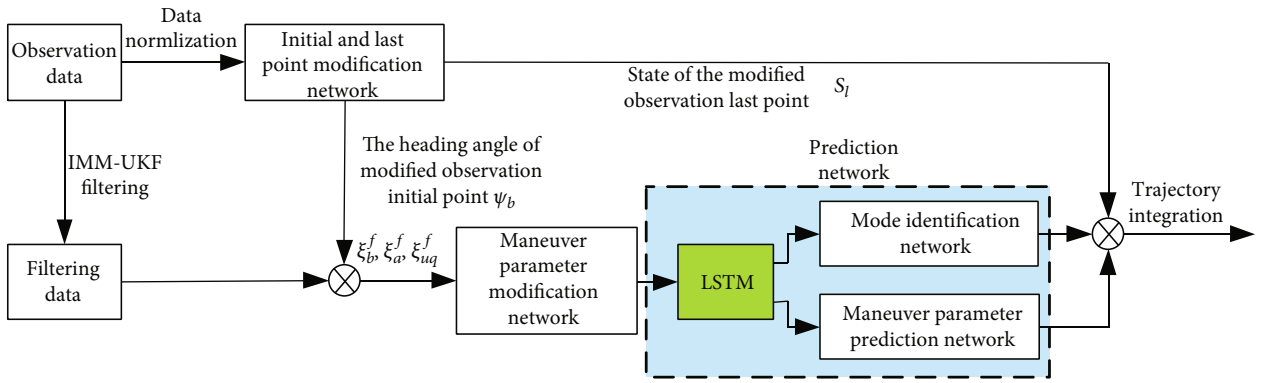

Figure 6: The prediction structure of the trajectory prediction based on the maneuver mode identification.

Table 2: Maneuver modes design formula.

Maneuver modes	Weaving maneuver	Turning maneuver	Equilibrium glide	Skip glide
Design formula	$l = l_0/2 + l_0/2 \cdot \sin(\omega b)$	$l = \mathrm{ab}^2$	$\dot{\theta} = 0$	$\alpha - v$

usually use the maximum lift-to-drag ratio angle of attack. The profile is as shown in

$$\alpha = \begin{cases} \alpha_{\max} V \geq V_1 \\ \dfrac{\alpha_K - \alpha_{\max}}{V_2 - V_1}(V - V_1) + \alpha_{\max} V_2 \leq V < V_1, \\ \alpha_K V < V_2 \end{cases} \tag{35}$$

where α_K is the maximum lift-drag ratio angle of attack, V_1 is the extreme points of speed beyond the constraint, and V_2 is the extreme points of speed within the constraint when the target selects maximum lift-to-drag ratio angle of attack.

In this paper, according to the method of reference [21], the attack angle corridor is used to limit the range of attack angle. And the CAV-H aircraft [36] is used to generate 5000 trajectories in all four modes meeting the constraints: weaving equilibrium glide, weaving skip glide, turning equilibrium glide, and turning skip glide. The generating trajectories are shown in Figure 7. According to Figure 7, all kinds of expected maneuver trajectories in longitudinal and lateral directions can be generated.

4.2. Simulation Conditions

4.2.1. Simulation Environment. Matlab and Python are used be the simulation environment. Pytorch framework is used for neural network training. Select Inter I7 as CPU and Geforce 2080TI as GPU in our simulation.

4.2.2. Data set. In this paper, the IMM-UKF algorithm [37] is used to track observed 20, 000 trajectories at the position (0.4°E, 0°N, 100). Assuming that the observational error of radar is Gaussian error with $[(30\mathrm{m})^2, (0.1°)^2, (0.1°)^2]$, the original trajectory data of all trajectories from 400 to 600 s are generated as observation data set and filtering data set. And the original trajectory data from 600 to 750 s are used as labels. The original trajectory data set and the maneuver parameter data set are used for the training and prediction of the initial and last point modification network, maneuver parameter modification network, and prediction network.

4.2.3. Training Conditions and Method. Each network took 100 trajectories as a batch and is trained 1000 epochs in total. The ADAM optimizer is used. And the training learning rate is 0.001 for the first 10 epochs and then adjusted to 0.0001.

To improve the robustness of the network, the observation data with a wider range of observational errors can be used to train the start and last point modification network. And dynamic models error can be added when generating the maneuver trajectory data set.

4.2.4. Definition of Error. In this paper, three types of errors usually used in trajectory prediction are selected: average error of spatial distance (AESD), final error of spatial distance (FESD), and maximum error of spatial distance (MESD). The definition is expressed as follows:

AESD is the average spatial distance between original trajectories and predicted trajectories

$$\mathrm{AESD} = \frac{\sum_i^N \sum_k^{L_p} \sqrt{\left(X_{\mathrm{pk}}^i - X_{\mathrm{tk}}^i\right)^2 + \left(Y_{\mathrm{pk}}^i - Y_{\mathrm{tk}}^i\right)^2 + \left(Z_{\mathrm{pk}}^i - Z_{\mathrm{tk}}^i\right)^2}/L_p}{N}. \tag{36}$$

FESD is the final spatial distance between original trajectories and predicted trajectories

$$\mathrm{FESD} = \frac{\sum_i^N \sqrt{\left(X_{\mathrm{pLp}}^i - X_{\mathrm{tLp}}^i\right)^2 + \left(Y_{\mathrm{pLp}}^i - Y_{\mathrm{tLp}}^i\right)^2 + \left(Z_{\mathrm{pLp}}^i - Z_{\mathrm{tLp}}^i\right)^2}}{N}. \tag{37}$$

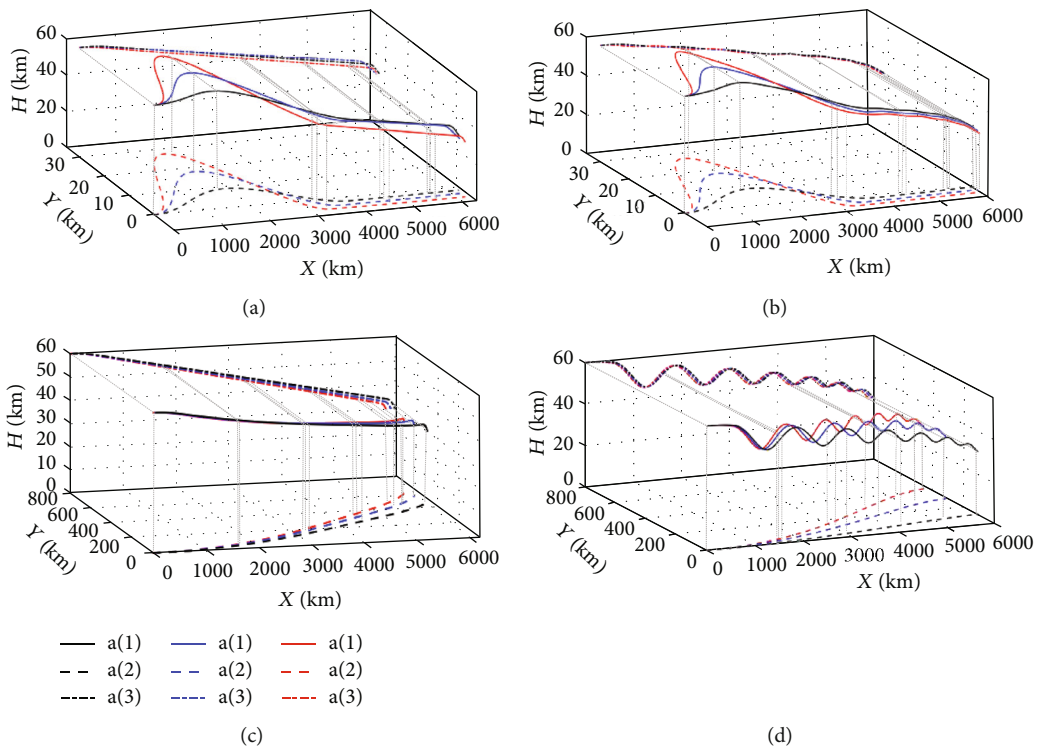

Figure 7: Example trajectory in different maneuver modes. (a) represents trajectories in weaving equilibrium glide. (b) represents trajectories in weaving skip glide. (c) represents trajectories in turning equilibrium glide. (d) represents trajectories in turning skip glide.

MESD is the maximum spatial distance between original trajectories and predicted trajectories.

$$\text{MESD} = \frac{\sum_i^N \max_k^{L_p} \sqrt{\left(X_{\text{pk}}^i - X_{\text{tk}}^i\right)^2 + \left(Y_{\text{pk}}^i - Y_{\text{tk}}^i\right)^2 + \left(Z_{\text{pk}}^i - Z_{\text{tk}}^i\right)^2}}{N}, \tag{38}$$

where N is the number of the test data set trajectories per maneuver mode. L_p is the length of predicted temporal sequence. $[X_{\text{pk}}^i, Y_{\text{pk}}^i, Z_{\text{pk}}^i]$ represent the predicted position at the time k of the $i-th$ test trajectory when $[X_{\text{tk}}^i, Y_{\text{tk}}^i, Z_{\text{tk}}^i]$ represent the real position.

4.3. Simulation Results

4.3.1. The Simulation Result of the Initial and Last Point Modification Network. According to analysis in Section 2.3, the large offset of the observation initial point can lead to a sharp increase of error for the trajectory prediction using integration. On the other hand, the start state of integration (the observation last point) has a great influence on trajectory prediction's precision. Especially the hypersonic target's path angle is small and close to 0, the instability of the observation last point may lead to a large longitudinal error of spatial distance as shown in Figure 8. For weaving equilibrium glide maneuver, the path angle of target should be unchanged, but the vibration of the observation last point without modification leads to trajectory integrated to the wrong direction, which obtains a large error of spatial distance. However, this problem can be solved better by using the start and last point modification network.

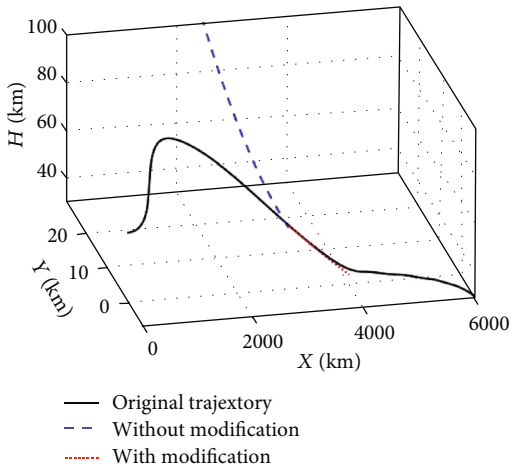

Figure 8: Comparison of predicted results with or without the start and last point modification network.

4.3.2. Result of Maneuver Parameter Modification Network. Since the filtering algorithm has limited suppression effect on noise, the prediction result based on maneuver parameters is easily affected by filtering the parameter's instability. As shown in Figure 9(a), in which the target is in the turning skip glide mode, there is a large gap between filtering parameters and original parameters, so it is difficult to fit the

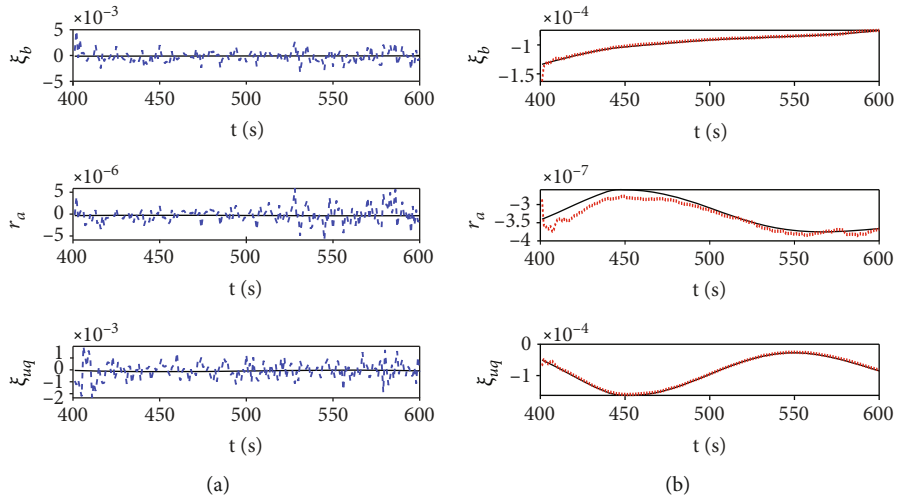

Figure 9: Result of parameter modification network. (a) is the variation of filtering maneuver parameters. (b) is the variation of filtering maneuver parameters.

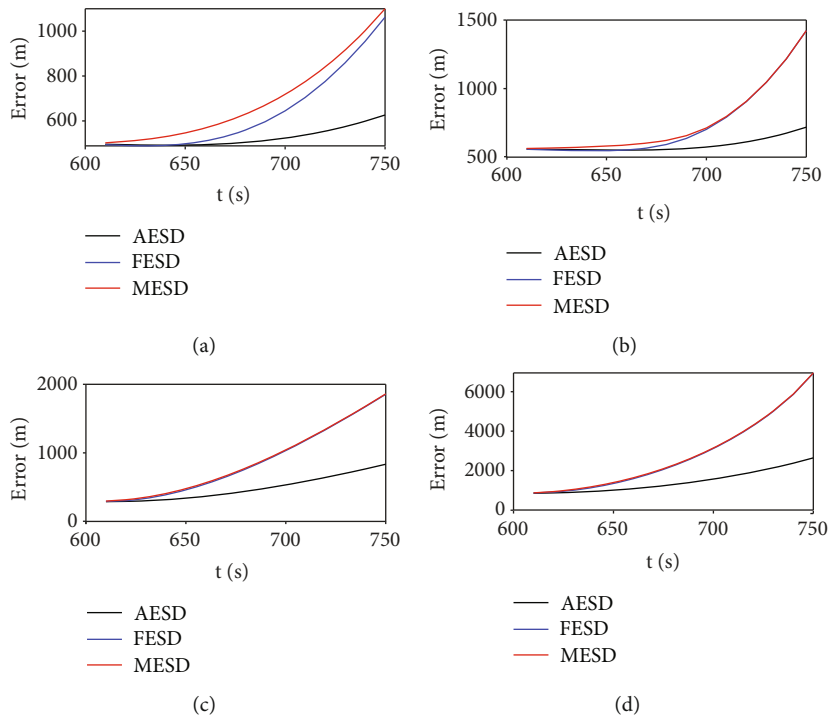

Figure 10: Variation of trajectory prediction's error. (a) is the prediction error in weaving equilibrium glide. (b) is the prediction error in weaving skip glide. (c) is the prediction error in turning equilibrium glide. (d) is the prediction error in turning skip glide.

original temporal sequence and predict the future temporal sequence of maneuver parameters. However, it can be seen from Figure 9(b) that the modified maneuver parameters can fit the original parameters accurately after using the parameter modification network. But the parameter's modification result is slightly worse in the early stage due to the influence of instable filtering parameter, while the fitting result is more accurate after LSTM modification in the late stage.

Variation of error in each maneuver mode is shown in Figure 10. It can be seen that the prediction errors in each maneuver mode increase gradually. And there exist certain errors in the prediction initial state, which is caused by the error of the baseline direction and position of the observation last point with the start and last point modification network. On the whole, the error in skip glide is greater than its equilibrium glide, and the error in turning maneuver mode is greater than its weaving maneuver mode. That means after identifying maneuver mode, the equilibrium glide has more prior knowledge and simpler model of maneuver parameters. Compared with the error in turning maneuver mode, the trajectories in weaving maneuvers are less affected by

Table 3: Prediction result in 150 s with and without parameter modification network.

Maneuver modes	LSTM-ξ_b, r_a, ξ_{uq}							
	Without parameters modification network				With parameters modification network			
	AESD (m)	FESD (m)	MESD (m)	Mode identification precision (%)	AESD (m)	FESD (m)	MESD (m)	Mode identification precision (%)
Weaving equilibrium glide	40, 818.62	123, 554.73	123, 555.30	17.82	626.39	1, 062.22	1, 099.51	98.63
Weaving skip glide	44, 307.53	159, 668.08	159, 668.08		718.68	1, 422.50	1, 423.32	
Turning Equilibrium glide	23, 863.16	170, 390.39	170, 394.72		834.20	1, 855.09	1, 861.15	
Turning skip glide	62, 592.56	62, 314.43	62, 314.426		2, 645.57	6, 936.62	6, 950.66	

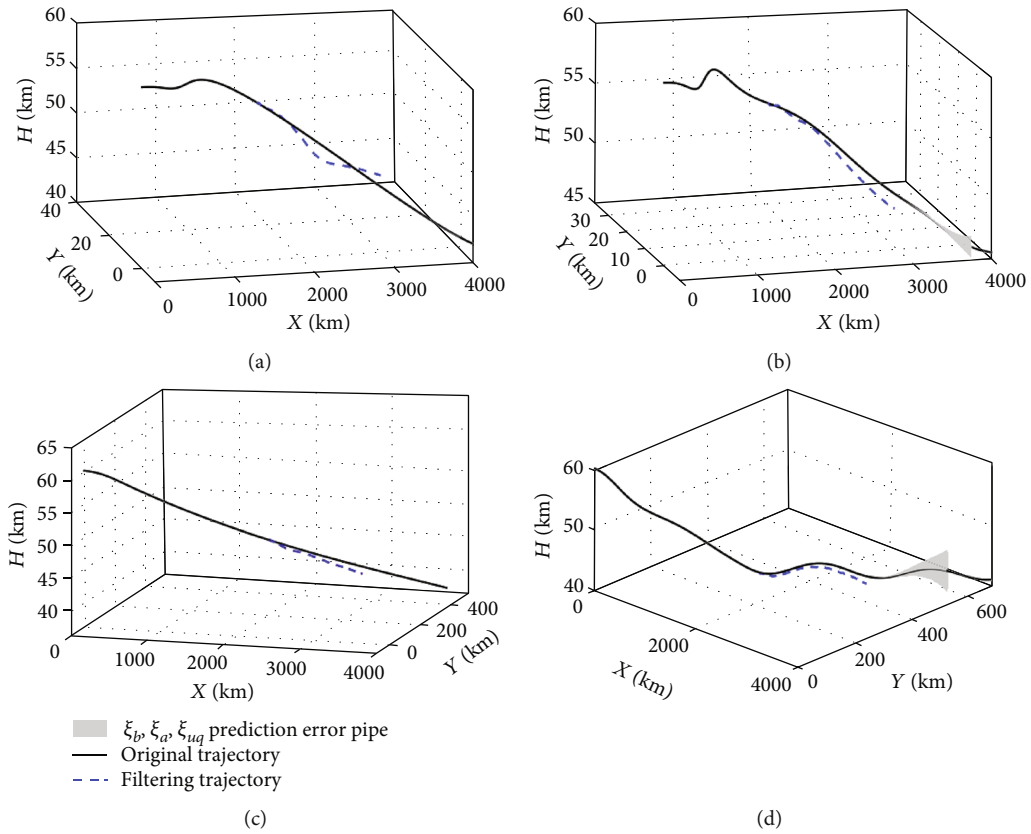

Figure 11: Prediction error pipe. (a) is the prediction error pipe in weaving equilibrium glide. (b) is the prediction error pipe in weaving skip glide. (c) is the prediction error pipe in turning equilibrium glide. (d) is the prediction error pipe in turning skip glide.

the error of baseline direction and have easily identified maneuver parameter temporal sequence. What is more, the trajectories in turning skip glide maneuver mode have the least use of prior knowledge and the most complex parameters sequence, which make the predicted trajectories in these modes to have the largest error and the fastest error accumulation speed. To show the advantage of the parameter modification network, the error in 150 s prediction trajectory with or without the parameter modification network is shown in Table 3.

From Table 3, the prediction precision of maneuver trajectories is greatly improved using parameter modification network, which is because the parameter instability brought by the filtering algorithm affects the prediction result of maneuver parameters seriously. For the overall prediction result, the error of equilibrium glide is smaller than that of skip glide. On the one hand, the longitudinal maneuver parameter sequence of equilibrium glide is more predictable. That means the prior information work up in improving the prediction accuracy. On the other hand, the error accumulation of turning skip glide is more serious when the parameter modification is not accurate enough, which leads to the overall error of turning skip glide is higher.

4.3.3. Result of Prediction Error Pipe. According to the maximum spatial distance for each direction in different

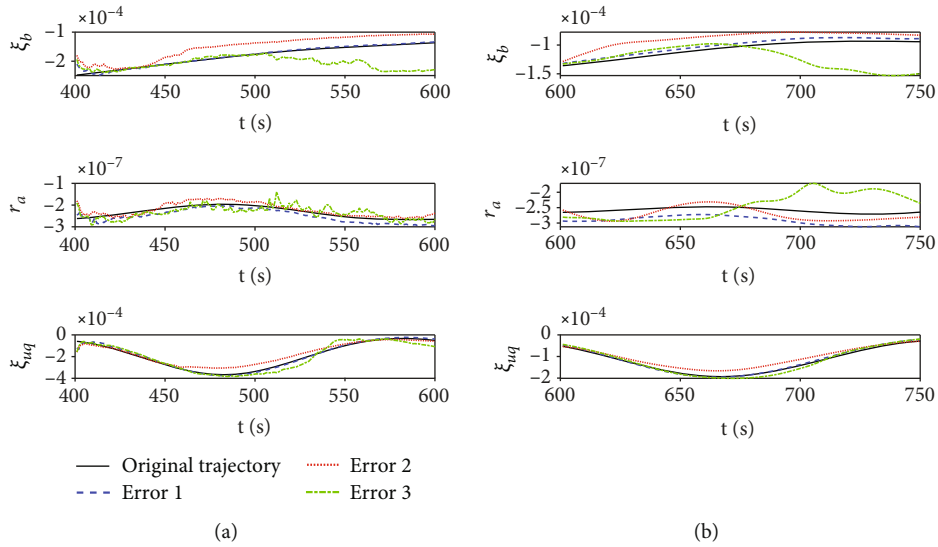

Figure 12: The variation of parameters with different error of observation. (a) is the variation of modified filtering maneuver parameters. (b) is the variation of predicted maneuver parameters.

prediction times, the prediction error pipelines within 150 s are shown in Figure 11, where (a), (b), (c),and (d), respectively, represent the error pipes for four types of maneuver trajectories: weaving equilibrium glide, weaving skip glide, turning equilibrium glide, and turning skip glide. By comparing (a) and (b) and (d) and (c), it can be seen that the width of the longitudinal error pipe of the skip glide is larger than that of the equilibrium glide when the longitudinal expansion speed of the pipe is faster. Comparing (b) with (d), it can be seen that the pipe expansion speed in the turning maneuver is faster than that in the weaving maneuver. The reason is that the prior information of the turning maneuver is less utilized when the parameter model in turning maneuver mode is more complex. As a whole, the prediction errors of hypersonic glide target in each maneuver mode are small, and the error pipeline based on it can provide information for interceptors effectively to achieve handover between midcourse and terminal guidance.

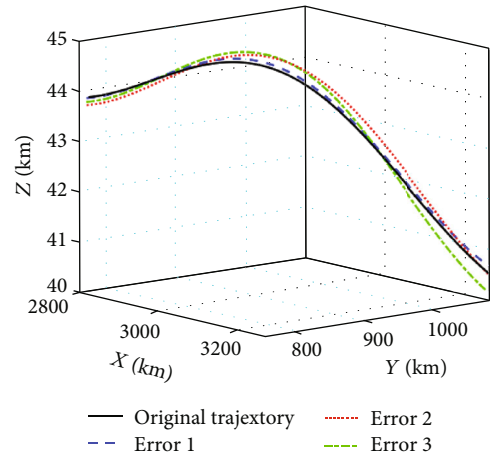

Figure 13: Predicted trajectory with different error of observation.

4.3.4. Analysis of the Effect for Trajectory Prediction of Observation Error. Since different observation errors of targets may affect the precision for trajectory prediction, several simulations to analyze the prediction effect with different radar observation errors are operated in this paper, in which the radar error parameters are $[(30\text{m})^2, (0.1^\circ)^2, (0.1^\circ)^2]$, $[(50\text{m})^2, (0.2^\circ)^2, (0.2^\circ)^2]$, and $[(100\text{m})^2, (0.5^\circ)^2, (0.5^\circ)^2]$. And the influence of the errors on the trajectory prediction is analyzed.

Take the most complex trajectory in turning skip glide mode as an example, as shown in Figures 12 and 13. error1, error2, and error3 in Figures 12 and 13 represent the trajectories with the above three radar error parameters, respectively. It can be seen from Figure 12, even though observation error increases, that the parameter modification network can still modify maneuver parameters effectively after using a filtering algorithm. It means the training method is valid to predict the noisy trajectory. However, a large observation error may lead to greater variation for the modified parameters, as shown in Figure 12(a). Besides, the modified parameters are passed through the maneuver parameter prediction network, and the variation law of maneuver parameters of the target can still be effectively estimated when its maneuver mode can also be identified. However, the variation of the modified parameters will lead to a large deviation of the predicted parameters, as shown in Figure 12(b).

On the other hand, a large observation error can lead to a large deviation of the modified last point position through the start and last point modification network, which will also have a certain impact on the trajectory prediction precision of the target as shown in Figure 13. In general, the method proposed in this paper is robust to the observation error when its mode identification accuracy can still reach 96.8% with a larger observation error. And when the method is applied, the error range of the radar is a knowable parameter, which can be analyzed and trained before using.

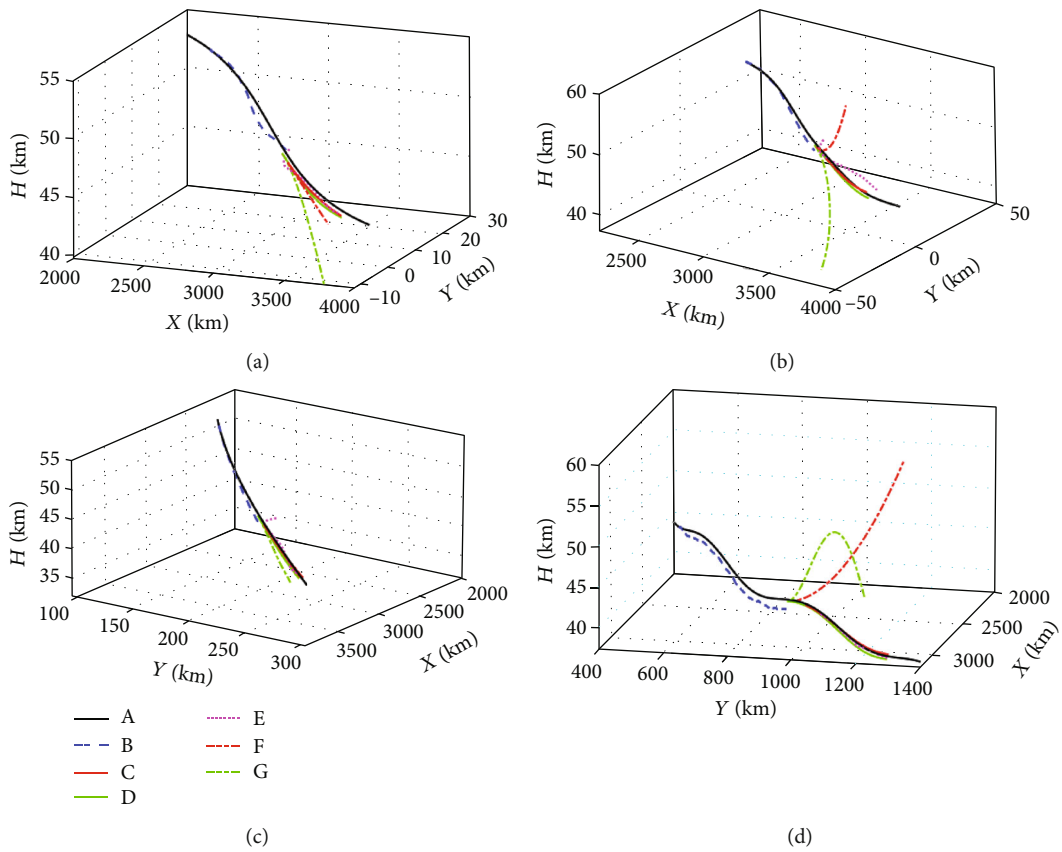

Figure 14: Comparison of prediction results for different methods. (a) is predicted trajectories in weaving equilibrium glide. (b) is predicted trajectories in weaving skip glide. (c) is predicted trajectories in turning equilibrium glide. (d) is predicted trajectories in turning equilibrium glide.

4.3.5. Comparison Results. The intelligent trajectory prediction algorithm based on maneuver mode identification in this paper is compared with the intelligent prediction method with aerodynamic parameters ξ_v, ξ_t, ξ_c, maneuver parameter ξ_b, r_a, ξ_{uq} fitting method, parameter ξ_v, ξ_t, ξ_c fitting method used in literature [22], and pure LSTM prediction method (in which the trajectory is predicted by using LSTM to estimate the target's flight state). The prediction result of various maneuver trajectories is shown in Figure 14. Figures 14, a and b represent the original trajectory and filtered trajectory; c is the prediction result of our method proposed in this paper; method d is the prediction result of the intelligent prediction method of parameters ξ_v, ξ_t, ξ_c; e and f are the prediction result of fitting parameters ξ_b, r_a, ξ_{uq} and ξ_v, ξ_t, ξ_c with simple function; and g is the result of pure LSTM method. (a), (b), (c), and (d), respectively, represent the prediction results in weaving equilibrium glide mode, weaving skip glide mode, turning equilibrium glide mode, and turning skip glide mode.

As can be seen from Figure 14, comparing the result of LSTM-ξ_b, r_a, ξ_{uq} with LSTM-ξ_v, ξ_t, ξ_c, our method has higher prediction precision in weaving maneuver mode and turning equilibrium maneuver. The season is the maneuver parameter sequence is more predictable, and more prior knowledge is obtained when the maneuver mode of target is identified. Compared with pure LSTM method, our method has smaller error and higher prediction precision. The season is the pure LSTM methods does not consider the dynamic model of the target in the process of prediction. Compared with methods e with f, it can be seen that the temporal sequence law of maneuver parameters ξ_b, r_a, ξ_{uq} is easier than aerodynamic parameter ξ_v, ξ_t, ξ_c to be fitted, which obtain better prediction result. What is more, by comparing the prediction result of our method with that of method e and f, it is found that the prediction error of method e and f is large. That means the temporal sequence law of maneuver parameters is influenced by the instability of filtering algorithm and cannot be accurately expressed by simple function. Fitting directly without modification will lead to inaccurate prediction results. The prediction errors of each method in 150 s are shown in Table 4.

As can be seen from Table 4, the best prediction precision can be mainly obtained through LSTM-ξ_b, r_a, ξ_{uq} algorithm proposed in this paper in several maneuver modes. AESD of our method in each mode does not exceed 2.6 km, and MESD does not exceed 6.9 km, with a pretty fast prediction speed.

During the simulation, there are several problems that affect the application of this method. Firstly, the observation

Table 4: Comparison of prediction results in 150 s for different methods.

Maneuver modes		Weaving equilibrium glide	Weaving skip glide	Turning equilibrium glide	Turning skip glide	Mean time of prediction(s)
LSTM ξ_v, ξ_t, ξ_c	AESD(m)	958.75	1, 384.02	1, 651.39	2, 893.55	0.0153
	MESD(m)	1, 631.40	2, 133.39	2, 682.99	6, 195.15	
LSTM ξ_b, r_a, ξ_{uq}	AESD(m)	626.39	718.68	834.120	2, 646.57	0.0156
	MESD(m)	1, 099.51	1, 423.32	1, 861.15	6, 950.66	
ξ_v, ξ_t, ξ_c Fitting	AESD(m)	59, 248.47	50, 351.25	178, 563.36	26, 832.49	0.0104
	MESD(m)	160, 146.41	129, 858.74	383, 113.43	93, 577.18	
ξ_b, r_a, ξ_{uq} Fitting	AESD(m)	2, 115.92	8, 535.19	1, 727.90	12, 912.31	0.0106
	MESD(m)	5, 678.43	26, 634.72	5, 038.86	39, 070.740	
Pure LSTM	AESD(m)	4, 837.72	4, 041.20	8, 633.52	3, 269.51	0.0085
	MESD(m)	8, 109.31	9, 658.73	18, 070.91	13, 616.74	

noise and dynamic models uncertain could lead to the failure of prediction. It is valid to train neural networks through trajectories data with the wider observation noise and dynamic models noise. By this way, the prediction precision is improved. And in order to solve this problem better, the intelligent filtering algorithm will be designed to learn more accurate parameter variation laws during tracking. Secondly, using complicate dynamic models to predict trajectory may lead to larger prediction error. It is found that the information of maneuver modes can be used to simply the dynamic equation. Through the maneuver mode identification, the more accurate predicted trajectory can be obtained.

5. Conclusion

In this paper, according to the trajectory characteristics of hypersonic glide target in various typical maneuver modes, a group of maneuver parameters suitable for maneuver mode identification is proposed. Through the analysis of parameters, it is verified that the maneuver parameters can keep characteristics in different maneuver modes. Based on it, the BLU coordinates at the observation start point are established, and its rationality has been analyzed. Then, combined with the maneuver parameters with LSTM, an intelligent trajectory prediction algorithm based on maneuver mode identification is proposed. Finally, the prediction result of the method is verified by the maneuver trajectory data set. The simulation results show that the maneuver mode identification precision of the proposed method can reach 98.63%, the average error of spatial distance is less than 2.64 km, and the maximum error of spatial distance is less than 6.95 km, which is better than the other comparison methods and can predict the trajectory of the hypersonic glide target accurately. And it also has a robustness to the observational error.

The proposed method could predict the trajectory of hypersonic glide target accurately when the maneuver modes of target do not change in the future time. It may not work well when the maneuver mode is different with the observation time. To handle this problem, the more prior information such as the intention of targets should be added. As a nonparter, the distribution of our strategic places and no-fly zones should be considered as prior information, and the model of importance map and association model between the strategic places and predicted trajectories can be designed. Based on these models, the trajectory prediction algorithm based on the intention inference of target will be researched in the future work.

Data Availability

The data sources from the references are all marked in this paper. And the parameters designed are all described in this paper. Therefore, the data in this paper can be fully obtained.

Conflicts of Interest

The authors declare that they have no conflicts of interest.

Acknowledgments

The authors would like to thank the Air and Missile Defense college of Air Force Engineering University of China for helpful discussions on topics related to this work. We thank the associate editor and the reviewers for their useful feedback that improved this paper. This study was supported by the National Natural Science Foundation of China (Grant no. 62173339 and no. 61873278).

References

[1] X. Yu, L. Liu, and G. Tang, "A reentry trajectory planning approach satisfying waypoint and no-fly zone constraints," in *Proceedings of 5th International Conference on Recent Advances in Space Technologies – RAST*, Istanbul, Turkey, 2011.

[2] C. Luo, H. Lei, J. Li, and C. Zhou, "A new adaptive neural control scheme for hypersonic vehicle with actuators multiple constraints," *Nonlinear Dynamics*, vol. 100, no. 4, pp. 3529–3553, 2020.

[3] C. R. Ruan, *The Optimal Trajectory of Aircraft Flying in the Air*, Astronautics Publishing Company, Beijing, 1978.

[4] L. O. Ferreira, *Nonlinear Dynamics and Stability of Hypersonic Reentry Vehicles*, University of Michigan, Michigan, 1995.

[5] X. Q. Chen, Z. X. Hou, J. X. Liu, and X. Q. Chen, "Phugoid dynamic characteristic of hypersonic gliding vehicles," *Science China: Information Sciences*, vol. 54, no. 3, pp. 542–550, 2011.

[6] P. Zarchan, "Proportional navigation and weaving targets," *Journal of Guidance, Control, and Dynamics*, vol. 18, no. 5, pp. 969–974, 1995.

[7] P. Zarchan, "Using filter banks to improve interceptor performance against weaving targets," in *AIAA Guidance, Navigation, and Control Conference and Exhibit*, Keystone, Colorado, 2006.

[8] T. R. Jorris and R. G. Cobb, "Multiple method 2-D trajectory optimization satisfying waypoints and no-fly zone constraints," *Journal of Guidance, Control, and Dynamics*, vol. 31, no. 3, pp. 543–553, 2008.

[9] T. R. Jorris and R. G. Cobb, "Three-dimensional trajectory optimization satisfying waypoint and no-fly zone constraints," *Journal of Guidance, Control, and Dynamics*, vol. 32, no. 2, pp. 551–572, 2009.

[10] G. Li, H. Zhang, and G. Tang, "Maneuver characteristics analysis for hypersonic glide vehicles," *Aerospace Science and Technology*, vol. 43, no. jun., pp. 321–328, 2015.

[11] D. R. Chapman, "An approximate analytical method for studying entry into planetary atmospheres," in *US Government Printing Office*, 1959.

[12] W. H. T. Roh, *Dynamics and Thermodynamics of Planetary Entry*, Prentice-Hall, Inc., Englewood Cliffs, N J, 1963.

[13] N. X. Vinh, E. K. Kim, and D. T. Greenwood, "Second-order analytical solutions for re-entry trajectories," in *AIAA Atmospheric Flight Mechanic Conference*, Monterey, CA, 1993.

[14] N. X. Vinh and Z. S. Kuo, "Improved matched asymptotic solutions for three-dimensional atmospheric skip trajectories," in *AIAA/AAS Astrodynamic Conference*, San Diego, CA, 1996.

[15] P. Lu, "Asymptotic analysis of quasi-equilibrium glide in lifting entry flight," *Journal of Guidance, Control, and Dynamics*, vol. 29, no. 3, pp. 662–670, 2006.

[16] I. M. Ross and F. Fahroo, "Legendre pseudospectral approximations of optimal control problems," in *Lecture Notes in Control and Information Sciences*, Springer, Berlin, Heidelberg, 2004.

[17] C. Y. Han and J. J. Xiong, "Method of trajectory prediction for unpowered gliding hypersonic vehicle in gliding phase," in *2016 IEEE Advanced Information Management, Communicates, Electronic and Automation Control Conference*, pp. 262–266, Xi'an, China, 2016.

[18] C. Han, J. J. Xiong, K. Zhang, and X. Lan, "Decomposition ensemble trajectory prediction algorithm for hypersonic vehicle," *Systems Engineering and Electronics*, vol. 40, no. 1, pp. 151–158, 2018.

[19] Q. Lei, L. Junlong, and Z. Di, "Tracking filter and prediction for nonballistic target HTV-2 in near space," in *The 27th Chinese Control and Decision Conference (2015 CCDC)*, pp. 3556–3561, 2015.

[20] C. Han and J. Xiong, "Method of trajectory prediction for unpowered gliding hypersonic vehicle in gliding phase," in *2016 IEEE Advanced Information Management, Communicates, Electronic and Automation Control Conference (IMCEC)*, pp. 262–266, Xi'an, China, 2016.

[21] L. I. Guanghua, *Motion Characteristics Analysis and Trajectory Prediction for Hypersonic Glide Vehicles*, National University of Defense Technology, 2016.

[22] Z. H. A. I. Dailiang, L. E. I. Humin, L. Jiong, and L. Tao, "Trajectory prediction of hypersonic vehicle based on adaptive IMM," *Acta Aeronautica et Astronautica Sinica*, vol. 37, no. 11, pp. 3466–3475, 2016.

[23] K. Liu, X. Hu, H. Zhou, L. Tong, W. D. Widanage, and J. Marco, "Feature analyses and modeling of lithium-ion battery manufacturing based on random forest classification," *IEEE/ASME Transactions on Mechatronics*, vol. 26, no. 6, pp. 2944–2955, 2021.

[24] K. Liu, X. Hu, J. Meng, J. M. Guerrero, and R. Teodorescu, "RUBoost-based ensemble machine learning for electrode quality classification in Li-ion battery manufacturing," *IEEE/ASME Transactions on Mechatronics*, pp. 1–10, 2021.

[25] F. A. Gers, J. Schmidhuber, and F. Cummins, "Learning to forget: continual prediction with LSTM," *Neural Computation*, vol. 12, no. 10, pp. 2451–2471, 2000.

[26] Z. Zou, Z. Shi, and Y. Guo, "Object detection in 20 years: a survey," 2019.

[27] R. W. Liu, M. Liang, J. Nie, W. Y. B. Lim, Y. Zhang, and M. Guizani, "Deep learning-powered vessel trajectory prediction for improving smart traffic services in maritime internet of things," *IEEE Transactions on Network Science and Engineering*, 2022.

[28] R. W. Liu, M. Liang, J. Nie et al., "STMGCN: mobile edge computing-empowered vessel trajectory prediction using spatio-temporal multi-graph convolutional network," *IEEE Transactions on Industrial Informatics*, p. 1, 2022.

[29] S. Wang, P. Zhao, B. Yu, W. Huang, and H. Liang, "Vehicle trajectory prediction by knowledge-driven LSTM network in urban environments," *Journal of Advanced Transportation*, vol. 2020, 20 pages, 2020.

[30] K. Liu, Y. Shang, Q. Ouyang, and W. D. Widanage, "A data-driven approach with uncertainty quantification for predicting future capacities and remaining useful life of lithium-ion battery," *IEEE Transactions on Industrial Electronics*, vol. 68, no. 4, pp. 3170–3180, 2021.

[31] K. Liu, Q. Peng, H. Sun, M. Fei, H. Ma, and T. Hu, "A transferred recurrent neural network for battery calendar health prognostics of energy-transportation systems," *IEEE Transactions on Industrial Informatics*, p. 1, 2022.

[32] C. Yuanli, Y. Deng, and S. Yuehua, "LSTM based trajectory classification and prediciton for hypersonic vehicle," in *The 21st Chinese Coference on System Simulation Technology and Application (CCSSTA21st)*, 2020.

[33] Y. Xie, X. Zhuang, Z. Xi, and H. Chen, "Dual-channel and bidirectional neural network for hypersonic glide vehicle trajectory prediction," *Access*, vol. 9, pp. 92913–92924, 2021.

[34] L. Sihao, "Trajectory prediction of hypersonic vehicles in near space based on neural," *Harbin Institute of Technology*, 2020.

[35] Y. Bin and H. Zhenghong, "Hypersonic vehicle track prediction based on GRNN," *Computer Applications and Software*, vol. 32, no. 7, pp. 239–243, 2015.

[36] T. H. Phillips, "A common aero vehicle (CAV) model," *Description, and Employment Guide.*, 2003.

[37] S. Li, H. Lei, L. Shao, and C. Xiao, "Multiple model tracking for hypersonic gliding vehicles with aerodynamic modeling and analysis," *IEEE Access*, vol. 7, pp. 28011–28018, 2019.